Geomech. Geophys. Geo-energ. Geo-resour. (2024) 10:8
https://doi.org/10.1007/s40948-023-00700-6

ORIGINAL ARTICLE

A novel evaluation method of natural gas hydrate saturation in reservoirs based on the equivalent medium theory

Qiangui Zhang · Quanshan Li · Xiangyu Fan · Yufei Chen · Zhaoxiang Wang · Bowei Yao · Na Wei · Jun Zhao

Received: 19 February 2022 / Accepted: 26 November 2023

Abstract Natural gas hydrate saturation (NGHS) in reservoirs is one of the critical parameters for evaluating natural gas hydrate resource reserves. Current widely-accepted evaluation methods developed for evaluating conventional natural gas saturation in reservoirs, to some extents, are not sufficient enough to obtain accurate predicted results. In light of the equivalent medium theory, the natural gas hydrate is regarded as the fluid (Mode A) when NGHS is relatively low, while it is regarded as the rock matrix (Mode B) when NGHS is high. Two mathematical model are then developed for evaluating NGHS at Mode A and B. Experimental verification shows that R^2 of the predicted results based upon the proposed model is 0.968, and the average absolute relative error percentage is 8.90%. The error of the predicted results gradually decreases with increasing NGHS, whereas increases with increasing confining pressure. In addition, the proposed model has been applied to the 142.9–147.7 m well section of Well DK-1 in the permafrost region, Qilian Mountains. The results show that the error of the predicted results is less than 13.92%, with its average error being 10.51%. The predicted value gradually increases with its error decreasing as the depth continues to increase, which is consistent with the change behavior of measured data. NGHS evaluation method proposed in this paper fully considers the occurrence form of natural gas hydrate in reservoirs. The model parameters are easy to determine and the predicted results are reliable.

Highlights

1. A new evaluation method of natural gas hydrate saturation is developed
2. The prediction error shows that $R^2 = 0.968$ and AAREP = 8.90% compared with test data
3. The predicted results of field application match the measured values well

Keywords Natural gas hydrate · Reservoir saturation · Equivalent medium theory · Evaluation method · Logging data

Q. Zhang (✉) · Q. Li · B. Yao · N. Wei
Petroleum Engineering School, Southwest Petroleum University, Chengdu 610500, Sichuan, China
e-mail: qgzhang@swpu.edu.cn

Q. Zhang · X. Fan · Y. Chen · N. Wei
State Key Laboratory of Oil and Gas Reservoir Geology and Exploitation, Southwest Petroleum University, Chengdu 610500, Sichuan, China

X. Fan · Y. Chen (✉) · J. Zhao
School of Geoscience and Technology, Southwest Petroleum University, Chengdu 610500, Sichuan, China
e-mail: yfchen@swpu.edu.cn

Z. Wang
CCDC Chang Qing Cementing Company, Xi'an 710000, Shanxi, China

Published online: 03 January 2024

List of symbols

S_g	Natural gas saturation (%)
S_h	Natural gas hydrate saturation (NGHS) in the reservoir (%)
K_h	Bulk modulus of natural gas hydrate (GPa)
K_w	Bulk modulus of water (GPa)
K_f	Bulk modulus of pore fluid in the reservoir (GPa)
K_{sat}	Bulk modulus of the equivalent medium of Mode A (GPa)
K_{dry}	Bulk modulus of dry rock (GPa)
ϕ	Porosity of the rock matrix in the reservoir without natural gas hydrate (%)
K_{ma}	Bulk modulus of the solid phase of rock in the reservoir (GPa)
ρ_b	Volume density of the reservoir (g/cm^3)
Δt_s	Shear wave (S-wave) time difference of the reservoir (μs/m)
Δt_c	Longitudinal wave (P-wave) time difference of the reservoir (μs/m)
a_c	Correction coefficient, $a_c = 1.0 \times 10^9$ GPa/(g/cm^3)
ϕ_c	Critical porosity of the reservoir (%)
P	Effective stress applied on rock in the reservoir (MPa)
r	Average number of particles in contact with the unit volume at the critical porosity (dimensionless)
G_{ma}	Shear modulus of rock matrix (MPa)
ν	Poisson' Ratio of rock matrix (dimensionless)
σ_{min}	Minimum in-situ stress in the vertical and two horizontal directions (MPa)
P_p	Formation pore pressure (MPa)
α	Boit elastic coefficient (dimensionless)
Δt_{mc}	Longitudinal wave (P-wave) time difference of the rock matrix (μs/m)
Δt_{ms}	Shear wave time difference of the rock matrix (μs/m)
ρ_m	Volume density of rock matrix (g/cm^3)
σ_v	Vertical stress in the reservoir (MPa)
H	Formation depth (m)
σ_h	Minimum horizontal stress in the reservoir (MPa)
σ_H	Maximum horizontal stress in the reservoir (MPa)
β_1, β_2	Tectonic stress coefficients (dimensionless)
ρ_f	Density of formation fluid (g/cm^3)
m	Number of minerals in the solid phase of rock (integer)
f_i	Volume fraction of the i-th mineral in the solid phase of rock (decimal)
K_i	Bulk modulus of the i-th mineral (MPa)
G_i	Shear modulus of the i-th mineral (MPa)
ϕ_r	Reservoir porosity when the natural gas hydrate is regarded as the rock matrix (%)
Δt_f	Longitudinal wave time difference of the reservoir fluid (μs/m)
ϕ_s	Sonic porosity before correction (%)
C_p	Reservoir compaction correction coefficient (decimal)
ξ	Model parameter for C_p (decimal)
λ	Correction coefficient for C_p (m^{-1})
ρ_i	Density of each mineral in the reservoir rock (g/cm^3)
ρ_h	Density of pure natural gas hydrate (g/cm^3)
ρ_w	Density of water (g/cm^3)
Shc	NGHS of the intersection point of the error curves of the predicted results calculated by Mode A and B
V_h	Longitudinal wave velocity of pure natural gas hydrate (m/s)
V_w	Longitudinal wave velocity of pure water (m/s)
V_m	Longitudinal wave velocity of rock matrix (m/s)
V_p	Longitudinal wave velocity of the natural gas hydrate reservoir (m/s)
V_{p1}	Longitudinal wave velocity calculated by wood equation (m/s)
V_{p2}	Longitudinal wave velocity calculated by the Time-average equation (m/s)
W	Weighting factor (dimensionless)
n	Constant related to natural gas hydrate saturation (dimensionless)
R^2	Regression R-square value (decimal)
D_p	Discrepancy percentage or relative difference (%)
AAREP	Average absolute relative error percentage (%)
N	Number of available observations (integer)
S_h^{test}	Observed test results of NGHS (%)
S_h^{pred}	NGHS predicted by models (%)
$E[\cdot]$	Expectation (or statistical mean) operator

1 Introduction

Natural gas hydrate saturation (NGHS) in reservoirs, generally, serves as a critical parameter for resource reserves calculation (Zhuo et al. 2021). The current evaluation methods of natural gas saturation in reservoirs are usually based on the resistivity or acoustic logging data, by establishing mathematical models in consideration of the characteristics of natural gas reservoirs, such as Archie formula (Azar et al. 2008), Lee weight equation (Lee 2002), Wood equation (Bao et al. 2022). However, due to the major discrepancy between natural gas hydrate reservoirs and conventional natural gas reservoirs, it is difficult to accurately evaluate NGHS in reservoirs using the traditional calculation methods. Therefore, it is of great importance to develop an evaluation method suitable for gas hydrate saturation in reservoirs, further to accurately evaluating the reservoir reserves.

Resistivity log data is commonly used for calculating the natural gas saturation (S_g) in reservoirs. For this method, it is generally considered that the rock pore space consists of only two substances: water and natural gas. The reservoir water saturation (S_w) is calculated by the relationship between the resistivity and water saturation of the reservoir, so as to calculate NGHS of the reservoir ($S_h = 1 - S_w$). This method was first proposed by Archie (2003) and developed by Poupon et al. (1954), Alger and Raymer (1963), etc., for conventional natural gas reservoirs. The most widely-used calculation models involve Simandoux formula (Simandou 1964), standard Archie formula (Kim et al. 2013), modified Archie formula (Riedel et al. 2013) and Indonesian formula (Amiri et al. 2012). However, Guo and Zhu (2011) pointed out that NGHS in reservoirs calculated by Archie's formula may pose some discrepancies compared with the actual saturation due to that the geological conditions considered in Archie's formula are different from those of the actual natural gas hydrate reservoirs. Thus, some novel models were developed with more considerations on the geological conditions for NGHS evaluation, such as the NGHS model considering gas hydrate as pore filling, particle support and separate stratification (Li et al. 2022a), the two-parameter calculation model of resistivity and acoustic interval transit time based on logging data (Li et al. 2022b), and the NGHS prediction method using joint inversion of resistivity and sonic logs (Pandey and Sain 2022). However, these models do not fully consider the natural gas hydrate states of solid as rock matrix, semisolid as filler and fluid during the decomposition process.

Sonic logging data is an effective information for evaluating NGHS in reservoirs (Ding et al. 2020). The most frequently-applied models using sonic logging data are developed via the correlation between rock composition, porosity, density and other parameters of the natural gas hydrate reservoir and the reservoir P-wave velocity. Leclaire et al. (1994) first used the Biot-Type equation to establish the relationship between the elastic wave velocity and reservoir gas saturation. For natural gas hydrates reservoirs, some mathematical models of NGHS in reservoirs based on the sonic velocity were developed in the past few years, such as the time-average equation (Wyllie et al. 1958; Pearson et al. 1983; Arun et al. 2018), the Wood equation (Bao et al. 2022), the BGTL model (Lee 2002), the KT equation (Kuster and Toksoz 1974; Zimmerman and King 1986), and the Frenkle-Gassmann equation (Zillmer 2006). Especially, the equivalent medium theory (Helgerud et al. 1999; Dvorkin et al. 1999), of which natural gas hydrate is considered to be part of the pore fluid when NGHS is low and is considered to be part of the rock matrix when NGHS is high, is mainly suitable for loose, high-porosity sediments. This model is widely accepted by scholars in the area of petroleum engineering (Ecker 2001; Liu et al. 2022). In addition, some empirical formulas were put forward to calculate the porosity of saturated water sediments, NGHS, free gas content, and seismic wave impedance, respectively, using the elastic wave impedance inversion technique based on the logging data (Lu and McMechan 2004). As well as, Zhu et al. (2023) developed a hydrate saturation evaluation according to the cementation factor and saturation index. Although some evaluation methods of NGHS in reservoirs have been developed using the sonic logging data, and some of them have been applied in the field measurement, these methods do not fully consider the characteristics of natural gas hydrate reservoirs, causing practical application to be challenging. Another drawback of these methods is that the parameters used to perform the evaluation are hard to obtain.

Furthermore, a few scholars drew upon mathematical deduction and seismic inversion to calculate NGHS in reservoirs. Shelander et al. (2012) proposed

a calculation method for computing NGHS based on seismic inversion, petrophysical models, and stratigraphic sequence in the absence of wells. Although these methods can be used to evaluate NGHS in a larger range of reservoirs, their accuracy are relatively low with little application potential in the accurate evaluation of reservoir reserves or the design of development parameters.

The above methods are mainly developed based on the calculation models used for conventional reservoirs, thus the typical reservoir characteristics of the natural gas hydrate and the easy-to-use calculation parameters have not been well considered in these methods, and the accuracy of the results predicted by these methods is still relatively low. Therefore, this paper, based on the equivalent medium theory, aims to fully consider the occurrence form of natural gas hydrate in the reservoir by two natural gas hydrate occurrence modes: 1) The lower-saturation natural gas hydrate in the reservoir is regarded as fluid (Mode A) whereas 2) the higher-saturation is regarded as matrix (Mode B). Based on the two modes, a calculation model for NGHS in reservoirs using logging data and core-testing data has been established to support and optimize the evaluation of natural gas hydrate resource reserves.

2 Calculation model of NGHS in reservoirs based on the equivalent medium theory

In the practical circumstances, the natural gas hydrate in reservoirs would have two occurrence forms (Helgerud et al. 1999; Ecker 2001; Fang et al. 2022), as shown in Fig. 1: (1) Mode A: moveable natural gas hydrate and, (2) Mode B: immovable natural gas hydrate. The natural gas hydrate of Mode A has not been fixed with the rock matrix and is regarded as a part of the pore fluid in reservoirs. Mode A is suitable for the case where NGHS of the reservoir is low. The natural gas hydrate of Mode B is fixed with the rock matrix, and in this case, natural gas hydrate and rocks form a reservoir rock matrix structure and the porosity of the reservoir will decrease. Mode B is suitable for the situation where NGHS of the reservoir is high. Therefore, according to the situations of two occurrence forms of natural gas hydrate, a new calculation model of NGHS in reservoir can be developed based on the equivalent medium theory and this model is introduced as follows.

2.1 Calculation model of NGHS in reservoirs for Mode A

The reservoir, including rock, water, gas and NGHS, is regarded as the equivalent medium of Mode A. Thus, based on the equivalent medium theory (Ecker 2001), NGHS in the reservoir can be expressed as:

$$S_{\mathrm{h}} = \frac{K_{\mathrm{w}}K_{\mathrm{h}} - K_{\mathrm{h}}K_{\mathrm{f}}}{K_{\mathrm{w}}K_{\mathrm{f}} - K_{\mathrm{h}}K_{\mathrm{f}}} \tag{1}$$

where S_{h} is the natural gas hydrate saturation (NGHS) in the reservoir, %; K_{h} is the bulk modulus of natural gas hydrate, GPa, which is 7.7 GPa (Dvorkin et al. 2003); K_{w} is the bulk modulus of water, GPa, which is 2.29 GPa (Lee 2004); and K_{f} is the bulk modulus of pore fluid in the reservoir, GPa.

In the Mode A, K_{f} can be computed by (Ecker 2001):

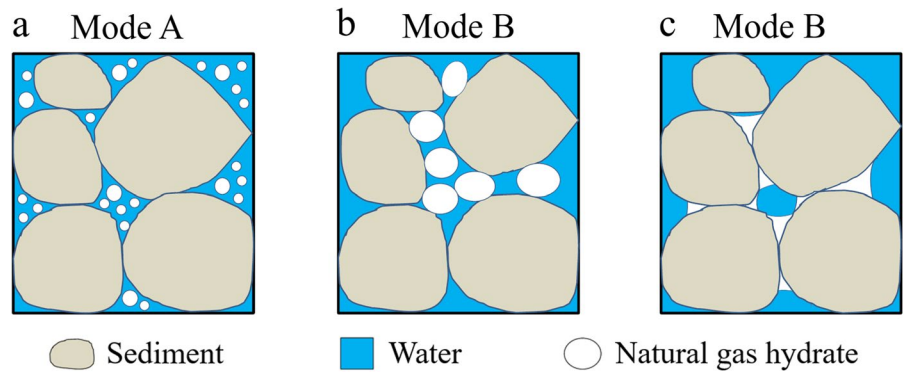

Fig. 1 Occurrence form schematic diagram of natural gas hydrate in reservoirs with moveable natural gas hydrate particles (**a**), with immovable natural gas hydrate particles (**b**), and with bonding natural gas hydrate blocks (**c**) (modified from Fang et al. 2022)

$$K_f = \frac{K_{ma}\phi\left(K_{dry} - K_{sat}\right)}{K_{sat}(1-\phi) - K_{sat}K_{dry}/K_{ma} - K_{ma} + (1+\phi)K_{dry}} \tag{2}$$

where K_{sat} is the bulk modulus of the equivalent medium of Mode A, GPa; K_{dry} is the bulk modulus of dry rock, GPa; ϕ is the porosity of the rock matrix in the reservoir without natural gas hydrate, %; and K_{ma} is the bulk modulus of the solid phase of rock in the reservoir, GPa.

Using the acoustic interval transit time data from well logging, the bulk modulus of the equivalent medium of Mode A (K_{sat}) can be easily obtained by Eq. (3) (Liu and Luo 2004).

$$K_{sat} = \rho_b \frac{3\Delta t_s^2 - 4\Delta t_c^2}{3\Delta t_s^2 \Delta t_c^2} \times a_c \tag{3}$$

where ρ_b is the volume density of the reservoir, g/cm^3, which can be obtained by density logging; Δt_s and Δt_c are the shear wave (S-wave) and longitudinal wave (P-wave) time difference of the reservoir, μs/m; a_c is the correction coefficient, ac = 1.0 × 10^{9}GPa/(g/cm^3).

Generally, only the longitudinal wave time difference of the reservoir can be obtained by well logging, and the shear wave time difference can be calculated by Eq. (4) (Liu and Luo 2004).

$$\Delta t_s = \frac{\Delta t_c}{1 - 1.15\left[\frac{(1/\rho_b)+(1/\rho_b)^3}{e^{(1/\rho_b)}}\right]^{1.5}} \tag{4}$$

In Eq. (2), K_{dry} can be obtained by Eq. (5) (Dvorkin et al. 1999).

$$K_{dry} = \begin{cases} \left[\dfrac{\phi/\phi_c}{K_{HM} + \frac{4}{3}G_{HM}} + \dfrac{1-\phi/\phi_c}{K_{ma} + \frac{4}{3}G_{HM}}\right]^{-1} - \dfrac{4}{3}G_{HM}, \ \phi < \phi_c \\ \left[\dfrac{(1-\phi)/(1-\phi_c)}{K_{HM} + \frac{4}{3}G_{HM}} + \dfrac{(\phi-\phi_c)/(1-\phi_c)}{\frac{4}{3}G_{HM}}\right]^{-1} - \dfrac{4}{3}G_{HM}, \ \phi \geq \phi_c \end{cases} \tag{5}$$

where,

$$K_{HM} = \left[\frac{r^2\left(1-\phi_c\right)^2 G_{ma}^2}{18\pi^2(1-\nu)^2}P\right]^{\frac{1}{3}} \tag{6}$$

$$G_{HM} = \frac{5-4\nu}{5(2-\nu)}\left[\frac{3r^2\left(1-\phi_c\right)^2 G_{ma}^2}{2\pi^2(1-\nu)^2}P\right]^{\frac{1}{3}} \tag{7}$$

where ϕ_c is the critical porosity of the reservoir, %, generally to be 36–40% (Nur et al. 1998); P is the effective stress applied on the rock in the reservoir, MPa; r is the average number of particles in contact with the unit volume at the critical porosity, generally to be 8–9.5 (Kuster and Toksoz 1974); G_{ma} is the shear modulus of the rock matrix, MPa; and ν is the Poisson' Ratio of the rock matrix, which can be calculated by Eq. (8) (Dvorkin et al. 1999).

$$\nu = \frac{0.5\left(K_{ma} - \frac{2}{3}G_{ma}\right)}{K_{ma} + \frac{G_{ma}}{3}} \tag{8}$$

The effective stress P applied on the rock in the reservoir is calculated by Eq. (9).

$$P = \sigma_{min} - \alpha P_p \tag{9}$$

where σ_{min} is the minimum in-situ stress in the vertical and two horizontal directions, MPa; P_p is the formation pore pressure, MPa; α is the Boit elastic coefficient, expressed as (Priestley 1999):

$$\alpha = 1 - \frac{\rho_b\left(\frac{3}{\Delta t_c^2} - \frac{4}{\Delta t_s^2}\right)}{\rho_m\left(\frac{3}{\Delta t_{mc}^2} - \frac{4}{\Delta t_{ms}^2}\right)} \tag{10}$$

where Δt_{mc} and Δt_{ms} are the longitudinal wave and shear wave time difference of the rock matrix, respectively, μs/m; ρ_m is volume density of rock matrix, g/cm^3, expressed as:

$$\rho_m = (1-\phi)\sum_{i=1}^{m} f_i \rho_i \tag{11}$$

The in-situ stresses in the three directions are calculated using Huang's model (Yin et al. 2017):

$$\begin{cases} \sigma_v = \rho_b g H \times 10^{-3} \\ \sigma_h = \left[\dfrac{\nu}{1-\nu} + \beta_1\right] \times \left(\sigma_v - \alpha P_p\right) + \alpha P_p \\ \sigma_H = \left[\dfrac{\nu}{1-\nu} + \beta_2\right] \times \left(\sigma_v - \alpha P_p\right) + \alpha P_p \end{cases} \tag{12}$$

Then σ_{min} is determined as follows:

$$\sigma_{min} = \min\left(\sigma_v, \sigma_h\right) \tag{13}$$

where σ_v is the vertical stress in reservoir, MPa; H is the formation depth, m; σ_h is the minimum horizontal stress in the reservoir, MPa; σ_H is the maximum horizontal stress in the reservoir, MPa; β_1 and β_2 are the tectonic stress coefficients, determined by the hydraulic fracturing experimental inversion method.

The formation pore pressure P_p is expressed as:

$$P_p = \rho_f g H \times 10^{-3} \tag{14}$$

where ρ_f is the density of the formation fluid, g/cm^3.

In Eqs. (2), (5), (6) and (7), K_{ma} and G_{ma} can be calculated by the following formulas (Ecker et al. 2001):

$$K_{ma} = \frac{1}{2}\left[\sum_{i=1}^{m} f_i K_i + \left(\sum_{i=1}^{m} \frac{f_i}{K_i}\right)^{-1}\right] \tag{15}$$

$$G_{ma} = \frac{1}{2}\left[\sum_{i=1}^{m} f_i G_i + \left(\sum_{i=1}^{m} \frac{f_i}{G_i}\right)^{-1}\right] \tag{16}$$

where m is the number of minerals in the solid phase of rock, integer; f_i is the volume fraction of the i-th mineral in the solid phase of rock, decimal, which can be obtained through the rock mineral composition test; and K_i and G_i are the bulk modulus and shear modulus of the i-th mineral, MPa, which are determined from the literature of Burland et al. (2012).

2.2 Calculation model of NGHS in reservoirs for Mode B

Natural gas hydrate is considered as a part of the rock matrix in Mode B, thus NGHS in reservoirs can be expressed as:

$$S_h = \frac{\phi - \phi_r}{\phi} \tag{17}$$

where ϕ_r is the reservoir porosity when the natural gas hydrate is regarded as the rock matrix, %.

According to the acoustic velocity data obtained by well logging, Eq. (18) is used to calculate the reservoir porosity (Liu et al. 2013):

$$\phi_r = \frac{\phi_s}{C_p} = \frac{\Delta t_c - \Delta t_{mc}}{\Delta t_f - \Delta t_{mc}} \cdot \frac{1}{C_p} \tag{18}$$

where Δt_f is the longitudinal wave time difference of the reservoir fluid, μs/m, generally to be 620 μs/m; ϕ_s is the sonic porosity before correction, %; C_p is the reservoir compaction correction coefficient, decimal, and C_p, which is widely accepted in petroleum engineering, can be written as the following empirical formula.

$$C_p = \xi - \lambda H \tag{19}$$

where ξ is the model parameter for C_p, decimal; λ is the correction coefficient for C_p, m^{-1}.

The volume density of the reservoir (ρ_b) can be expressed as:

$$\rho_b = (1-\phi)\rho_i + \left(\phi - \phi_r\right)\rho_h + \phi_r \rho_w \tag{20}$$

where ρ_i is the density of each mineral in the reservoir rock, g/cm^3, which can be obtained by checking the literature of Burland et al. (2012); ρ_h is the density of pure natural gas hydrate, g/cm^3, which is taken as 0.9 g/cm^3; ρ_w is the density of water, g/cm^3, which is taken as 1.0 g /cm^3.

Thus, according to Eqs. (11) and (20), we have:

$$\phi = \frac{\sum_{i=1}^{m} f_i \rho_i - \phi_r \rho_h + \phi_r \rho_w - \rho_b}{\sum_{i=1}^{m} f_i \rho_i - \rho_h} \tag{21}$$

2.3 Method for selecting Mode A or B

The calculation formulas of NGHS in reservoirs of both Mode A and Mode B are given above. For the actual application, the selection of Mode A or B is carried out through the following steps, as shown in Fig. 2.

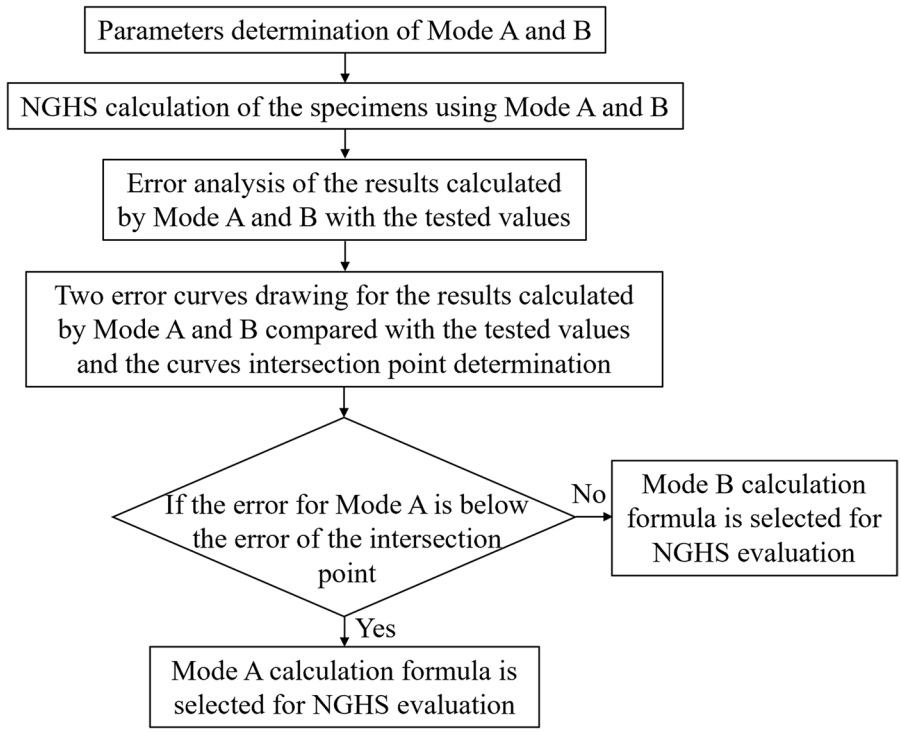

Fig. 2 Flow chart of the selection of Mode A or B for NGHS evaluation

(1) The parameters of both Mode A and Mode B are obtained for the same rock specimen prepared under different NGHSs.
(2) Using the parameters for the same rock specimen prepared under different NGHSs, NGHSs in the rock specimen are calculated by the calculation formulas of both Mode A and Mode B.
(3) The predicted results by the calculation formulas of both Mode A and Mode B are compared with the measured values, and the errors of the predicted results by the calculation formulas of both Mode A and Mode B can be obtained.
(4) The error curves of the predicted results calculated by Mode A and B are drawn as a figure, and an intersection point for the two curves can be obtained. Thus, we can determine that Mode A calculation formula is selected for NGHS evaluation while the errors of the predicted results calculated by Mode A is below the value of the intersection point, whereas the Mode B calculation formula is selected for NGHS evaluation while the errors of the predicted results calculated by the Mode A is higher than the value of the intersection point.

The NGHS of the intersection point (Shc) is, therefore, the critical value for selecting whether Model A or Model B to evaluate NGHS in the rock specimen. This critical NGHS is a constant value for rocks no matter how the size or number of rock pores and stress environment vary. This is due to that the ratio of the removable natural gas hydrate in the rock pores, which is the critical NGHS, is the same no matter how the size of rock pores varies.

3 Evaluation of the proposed model

3.1 Other common models for comparison

Two widely-accepted prediction models for natural gas saturation in reservoirs are briefly presented to compare with the proposed model.

3.1.1 Wood equation

The Wood equation has better applicability for evaluating the saturation of the suspended pore fluid filled in the rock pores with higher saturation, and the NGHS model derived by Wood equation is expressed as (Bao et al. 2022):

$$S_h = \left(\frac{\phi_r}{\rho_{\mathrm{w}} V_{\mathrm{w}}^2} + \frac{1-\phi_r}{\rho_{\mathrm{m}} V_m^2} - \frac{1}{\rho_b V_p^2} \right) \frac{\rho_w \rho_h V_w^2 V_h^2}{\phi_r (\rho_h V_h^2 - \rho_{\mathrm{w}} V_w^2)} \tag{22}$$

where V_{h}, V_{w}, V_{m}, and V_{p} are the longitudinal wave velocities of pure natural gas hydrate, pure water, rock matrix, and natural gas hydrate reservoir, respectively, m/s; the longitudinal wave velocity of pure natural gas hydrate (V_{h}) is 3650 m/s, and the longitudinal wave velocity of pure water (V_{w}) is 1500 m/s.

3.1.2 Weight equation

Weight equation is developed based on Time-average equation (Lee et al. 1996) and Wood equation (Bao et al. 2022). A weight factor (W) and a constant (n) are used to correct the predicted result to adapt to the actual situation. The expression of Weight equation is as follows:

$$S_{\mathrm{h}} = 1 - \left[\frac{V_{\mathrm{p1}} V_{\mathrm{p2}} - V_{\mathrm{p}} V_{\mathrm{p1}}}{W\phi \left(V_{\mathrm{p}} V_{\mathrm{p2}} - V_{\mathrm{p}} V_{\mathrm{p1}} \right)} \right]^{\frac{1}{n}} \tag{23}$$

where V_{p1} is the longitudinal wave velocity calculated by Wood equation, m/s; V_{p2} is the longitudinal wave velocity calculated by the Time-average equation, m/s; W is the weight factor, dimensionless, generally being equal to 1; and n is the constant related to NGHS, dimensionless, generally equal to 32.

3.2 Criteria for performance comparison

We used three different error measurements to assess the validity of predictions computed by different models: the regression R-square value (R^2), the discrepancy percentage or relative difference (D_{p}), and the average absolute relative error percentage (AAREP). AAREP is preferably used below because it is a simple estimator that provides a direct indication of the prediction error. Their definitions are (Shen et al. 2012a, b, 2014; Zhang et al. 2021a, 2023):

$$R^2 = 1 - \frac{\sum_{i=1}^{N} \left(S_{\mathrm{h},i}^{\mathrm{test}} - S_{\mathrm{h},i}^{\mathrm{pred}} \right)^2}{\sum_{i=1}^{N} \left(S_{\mathrm{h},i}^{\mathrm{test}} - E\left[S_{\mathrm{h},i}^{\mathrm{test}} \right] \right)^2} \tag{24}$$

$$D_{\mathrm{p},i}[\%] = \frac{S_{\mathrm{h},i}^{\mathrm{pred}} - S_{\mathrm{h},i}^{\mathrm{test}}}{S_{\mathrm{h},i}^{\mathrm{test}}} \times 100\% \tag{25}$$

$$\mathrm{AAREP}[\%] = \frac{\sum_{\mathrm{i}=1}^{\mathrm{N}} \left| D_{\mathrm{p,i}} \right|}{N} \tag{26}$$

where N is the number of available observations, integer; $S_{\mathrm{h}}^{\mathrm{test}}$ is the observed test results of NGHS, %; $S_{\mathrm{h}}^{\mathrm{pred}}$ is the NGHS predicted by models; and $E[\cdot]$ denotes the expectation (or statistical mean) operator.

Based on the above definitions, it is clear that a smaller AAREP corresponds to a more reliable model. Meanwhile, R^2 increases with the quality of the predictions, so that higher R^2 values correspond to models with lower AAREP values. $D_{p,i}$, that is needed to compute AAREP, is the relative difference between predicted and observed values for the i-th test.

3.3 Experimental data and model parameters

The experimental data of NGHS and acoustic wave velocity is tested by the SHW-III natural gas hydrate acousto-electricity test device for the specimens of loose natural gas hydrate deposits with different NGHSs. These tests were conducted under triaxial uniform stress (σ_{min}) of 10 MPa, 15 MPa and 20 MPa, respectively. NGHS of the specimen is calculated based on the material balance equation (Sun et al. 2018) and the PVT equation of state (Zhang et al. 2015), and the acoustic wave velocity in the specimen is tested directly by the device. NGHSs and acoustic wave velocities for the same specimen were tested after each gas injection, and the experimental data is shown in Table 1 (Zhao et al. 2018).

According to the test results presented in Table 1 and other rock petrophysics experiments, the parameters of three comparison models can be

Table 1 Experimental data of NGHS and acoustic wave velocity (Zhao et al 2018)

Gas injection step	$\sigma_{min}=20$ MPa				$\sigma_{min}=15$ MPa				$\sigma_{min}=10$ MPa			
	S_h (%)	V_p (m/s)	V_s (m/s)	ρ_b (g/cm^3)	S_h (%)	V_p (m/s)	V_s (m/s)	ρ_b (g/cm^3)	S_h (%)	V_p (m/s)	V_s (m/s)	ρ_b (g/cm^3)
1th	5.35	3705	1985	2.352	1.79	2542	1356	2.352	6.50	2017	851	2.351
2nd	27.96	4062	2068	2.351	13.84	2779	1536	2.351	11.96	2175	885	2.352
3rd	55.36	4479	2212	2.351	28.98	3113	1715	2.352	29.10	2580	975	2.353
4th	72.13	5257	2404	2.353	56.61	3945	2084	2.353	42.44	2792	7084	2.352
5th	77.83	5479	2681	2.354	69.37	4095	2194	2.354	57.78	3365	1584	2.354
6th									68.07	3589	1743	2.354

Table 2 Basic model parameters

σ_{min} (MPa)	ϕ (%)	C_p	K_{ma} (MPa)	G_{ma} (MPa)	ρ_m (g/cm^3)	ϕ_c	r	Δt_{mc} (μs/m)	f_i	P_p (MPa)	ν
10	36.0	2.04	5.789×10^4	2.7×10^4	2.65	0.368	9.5	168	1	4	0.298
15	28.4	1.77				0.36	9				
20	13.0	1.72				0.4	9.5				

obtained using the method mentioned in Sect. 2, as shown in Tables 2 and 3. ϕ is measured by the mercury intrusion method using an automatic mercury porosimeter of PoreMaster60 (manufactured by Quantachrome Instruments, USA). C_p is determined by the comparison between ϕ and the porosity determined by the velocity of longitudinal wave, using Eq. (18). The data used for calculating ϕ_s are the velocities at longitudinal wave of 500.08 μs/m, 395.20 μs/m, 295.25 μs/m for the condition of $\sigma_{min}=10$ MPa, 15 MPa and 20 MPa, respectively. K_{ma}, G_{ma} and ρ_m of quartz sand are determined from the literature written by Burland et al. (2012). Changes in ρ_b with the gas injection time are measured by theoretical calculation by the mass of rock, water and gas, as shown in Table 1. ϕ_c and r are determined from the literature authored by Nur et al. (1998) and Kuster and Toksoz (1974), respectively.

3.4 Results and analysis

Experimental data and model parameters mentioned in Sect. 3.3 are substituted into the proposed model of both Mode A and Mode B, and NGHSs of the specimen after different gas injection steps are calculated. The errors of the predicted results for the Mode A and B under the triaxial uniform stress (σ_{min}) of 10 MPa and 15 MPa with measured saturations are shown in Fig. 3. There is an intersection point between the two error curves of Mode A and B predicted results. The prediction errors of the intersection points are 8.09% and 8.11% for the conditions of triaxial uniform stress (σ_{min}) of 10 MPa and 15 MPa, respectively. When the measured saturation is lower than the NGHS of the intersection point, the prediction error of Model A is significantly lower than that of Model B; when the measured saturation is higher than the NGHS of the intersection point, the prediction error of Model B is significantly lower than that of Model A. The similar NGHS of the intersection point can also demonstrate that this value would not change with the size and number of rock pores, as well as the stress condition of rock, as mentioned in Sect. 2.3. Therefore, we can determine the NGHS of the intersection point as 8.10% (average value of 8.09% and 8.11%), that is, if NGHS is lower than 8.10%, the calculation model of Mode A would be used for NGHS evaluation, whereas the calculation model of Mode B would be used when NGHS is higher than 8.10%.

The errors of the predicted results by the proposed model changed with the measured saturation and the triaxial uniform stress, as shown in Fig. 4. From Fig. 4a, it can be seen that the error of the predicted results changes a lot under σmin = 10 MPa, and the error of the predicted results shows a relatively stable

Table 3 Other model parameters

σ_{min} (MPa)	Gas injection step	Δt_c (μs/m)	Δt_s (μs/m)	α	P (MPa)	K_{sat} (MPa)	K_{HM} (MPa)	G_{HM} (MPa)	K_{dry} (MPa)	K_f (MPa)	S_h (Mode A) (%)	S_h (Mode B) (%)
10	1th	495.786	1175.088	0.695	7.128	7291.316	1294.509	1728.635	1369.612	2394.779	6.23	1.29
	2th	459.770	1129.944	0.638	7.447	8662.864	1308.066	1746.738	1383.905	2993.778	33.46	12.14
	3th	387.597	1025.641	0.471	8.116	12,663.915	1346.089	1797.512	1423.990	4863.910	75.32	33.87
	4th	358.166	922.509	0.389	8.446	14,637.028	1364.074	1821.529	1442.948	5859.844	86.71	42.74
	5th	297.177	631.313	0.217	9.132	18,747.870	1400.093	1869.627	1480.909	8112.674	102.15	61.10
	6th	278.629	573.723	0.133	9.467	20,750.728	1416.991	1892.192	1498.716	9307.423	107.31	66.69
15	1th	393.391	737.463	0.833	11.667	9423.773	1477.743	1973.318	2484.350	2359.322	4.18	0.80
	2th	359.842	651.042	0.810	11.761	10,756.216	1481.713	1978.619	2490.789	2863.679	28.51	15.56
	3th	321.234	583.090	0.760	11.959	13,557.469	1489.990	1989.672	2504.210	3989.235	60.63	32.56
	4th	253.485	479.846	0.594	12.625	22,964.867	1517.135	2025.920	2548.189	8566.035	104.28	62.37
	5th	244.200	455.789	0.570	12.721	24,324.483	1520.978	2031.053	2554.412	9353.230	107.48	66.46
20	1th	269.892	503.790	0.648	17.409	19,916.277	1676.909	2239.276	9391.778	2387.060	5.79	0.96
	2th	246.210	483.559	0.551	17.795	25,366.402	1689.200	2255.689	9448.704	4090.722	62.65	24.44
	3th	223.251	452.080	0.437	18.251	31,818.704	1703.524	2274.817	9514.865	6799.779	94.40	47.20
	4th	190.212	415.973	0.171	19.314	46,843.717	1735.976	2318.153	9664.057	19,936.651	125.98	79.96
	5th	182.521	372.995	0.151	19.398	48,019.442	1738.465	2321.476	9675.457	21,853.474	127.41	87.59

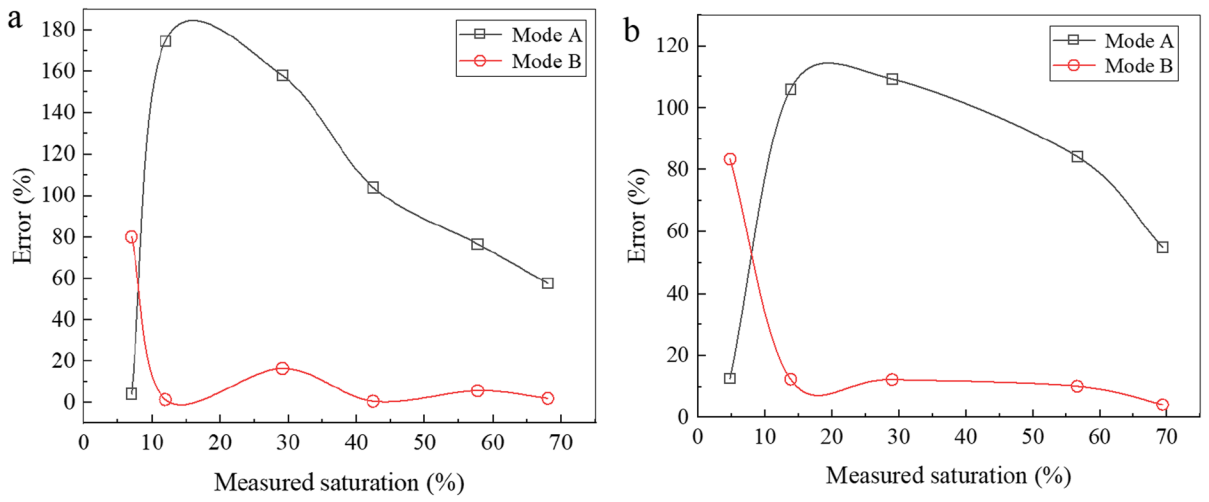

Fig. 3 Prediction error and measured saturation curves of Model A and B: **a** $\sigma_{min} = 10$ MPa; **b** $\sigma_{min} = 15$ MPa

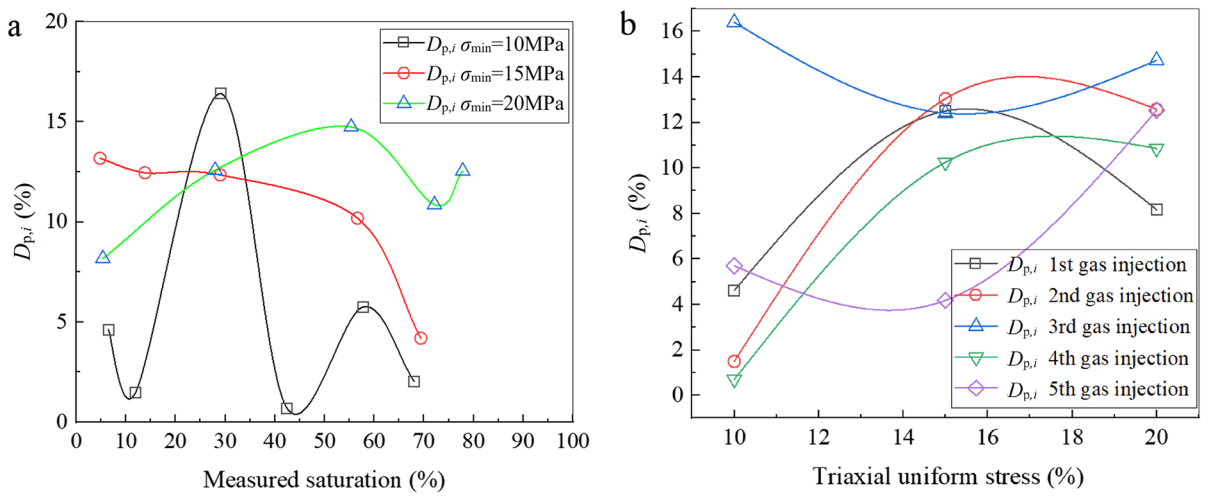

Fig. 4 Errors of the predicted results by the proposed model changed with the measured saturation (**a**) and the triaxial uniform stress (**b**)

variation under σmin = 15 MPa and 20 MPa. This implies that the prediction accuracy is highly affected by triaxial uniform stress. The error of the predicted results for Mode B generally decreases with increasing measured saturation. For example, the average errors are 9.04%, 14.51%, 7.27%, and 7.49% respectively at the 2nd, 3rd, 4th and 5th injections. The reason for this would be explained as follows: when NGHS is relatively low, some part of the natural gas hydrate with poor bonding strength (as shown in the Fig. 1b) has a weaken propagation capacity in response to the acoustic wave. In this case, the measured acoustic velocity is relatively low. Therefore, some natural gas hydrate particles embedded in rock particles are regarded as water in the model calculation. However, the measured saturation is calculated based on the material balance equation and the PVT equation of state as mentioned in Sect. 3.3, in which situation these natural gas hydrate particles is accurately determined as natural gas hydrate particles. Therefore, considering that the ratio of the natural gas hydrate with poor bonding strength would decrease

Table 4 Natural gas hydrate saturation predicted by the three models and its associated error analysis

P_c (MPa)	Number of gas injection	Test results (%)	Predicted results by the proposed model (%)		Predicted results by Wood equation (%)		Predicted results by Lee weight equation (%)	
			Value	Error	Value	Error	Value	Error
10 MPa	1	6.50	6.20	4.62	36.56	462.42	7.00	7.69
	2	11.96	12.14	1.50	40.96	242.50	14.00	17.06
	3	29.10	33.87	16.40	49.67	70.69	31.00	6.53
	4	42.40	42.74	0.70	53.14	25.22	39.50	6.93
	5	57.80	61.10	5.75	60.00	3.85	55.00	4.81
	6	68.10	66.69	2.03	61.91	9.05	66.00	3.04
	Average error (%)			5.16		27.20		7.68
15 MPa	1	4.80	4.20	12.50	58.55	1119.70	6.30	31.25
	2	13.80	15.60	13.04	61.98	349.17	22.00	59.42
	3	29.00	32.60	12.41	65.82	126.98	40.00	37.93
	4	56.60	62.40	10.25	71.75	26.76	50.00	11.66
	5	69.40	66.50	4.18	72.36	4.26	61.00	12.10
	Average error (%)			10.48		52.67		30.45
20 MPa	1	5.35	5.79	8.17	60.02	1021.93	6.20	15.89
	2	27.96	24.44	12.58	65.58	134.56	32.00	14.45
	3	55.36	47.20	14.73	76.70	38.55	51.00	7.88
	4	72.13	79.96	10.86	54.11	24.99	80.00	10.91
	5	77.83	87.59	12.54	43.16	44.55	75.00	3.64
	Average error (%)			11.78		60.66		10.55
Total average error (%)				9.14		46.84		15.70

with increasing gas injection time (increasing NGHS), the accuracy of predicted results for Mode B will increase with increasing NGHS.

The error of the predicted results increases with increasing triaxial uniform stress, as shown in Fig. 4b. For example, Dp,i is 0.7–16.4% with an average value of 5.16% for $\sigma_{min} = 10$ MPa; Dp,i is 4.18–13.04% with an average value of 10.48% for $\sigma_{min} = 15$ MPa; and Dp,i is 8.71–14.73% with an average value of 11.78% for $\sigma_{min} = 20$ MPa. The reason can be described as follow. The rock porosity (ϕ) would change with increasing triaxial uniform stress, but this rock porosity (ϕ) is set as a constant value in the proposed model. In this case, a higher triaxial uniform stress would cause a larger change of rock porosity (ϕ), resulting in a bigger error of the predicted results. However, the effect of stress on the rock porosity is negligible due to that the volumetric strain of rock is usually lower than 1.5% before failure (Qiu et al. 2019), resulting in a relatively small change of the errors of the predicted results under different triaxial uniform stress.

The predicted results of the proposed model, Wood equation and Weight equation and the error of the predicted results compared with measured saturations are shown in Table 4. We can clearly find that the predicted results by the proposed model agree better with the measured saturation compared with other two models. This can be verified by the total average errors of 9.14%, 46.84% and 15.70% for the proposed model, Wood equation, and Weight equation, respectively.

The comparison of the predicted results of the models and the measured saturations (Fig. 5) also shows that the proposed model has higher prediction accuracy compared with other two models. This can be certified by the following data: AAREP and R^2 of the predicted results by the proposed model, Weight equation, Wood equation are 8.90% and 0.968, 15.69% and 0.958, 55.70% and 0.472, respectively. In addition, the error of the predicted results for Weight equation is just a little higher than that for the proposed model and much lower than that for

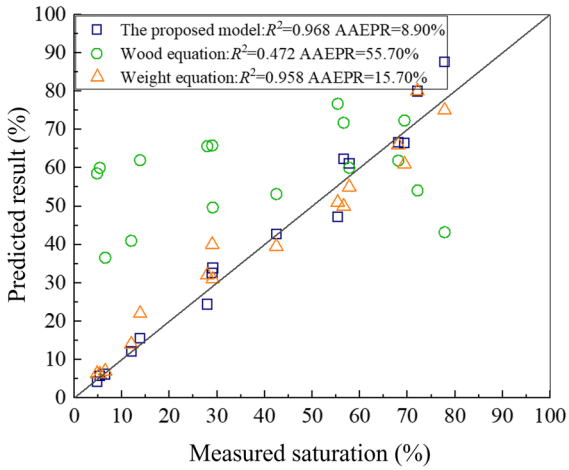

Fig. 5 Comparison of the predicted results of the models and the measured saturations

Wood equation. This would be due to that Weight equation is developed based on Time-average equation and Wood equation, and the prediction accuracy of Weight equation has been enhanced by the weight factor (W) and the constant (n) compared with the prediction accuracy of Wood equation.

4 Field application

4.1 Background

The proposed model is used to evaluate NGHS of a reservoir well section of the DK-1 scientific drilling test well, located in Muli Depression of the permafrost region of Qilian Mountains, northeast of the Qinghai-Tibet Plateau, China. This area can be divided into three tectonic units: the southern Qilian tectonic belt, the northern Qilian tectonic belt and the central Qilian block, as shown in Fig. 6 (Lu et al. 2010). The permafrost region of Qilian Mountains covers an area of 10×10^4 km^2, and its annual average ground temperature is 1.5–2.4 °C. The thickness of the frozen formation of the permafrost region is 50–139 m (Zhang et al. 2021b). This implies that the conditions of temperature and pressure are highly suitable for the reservoir-forming

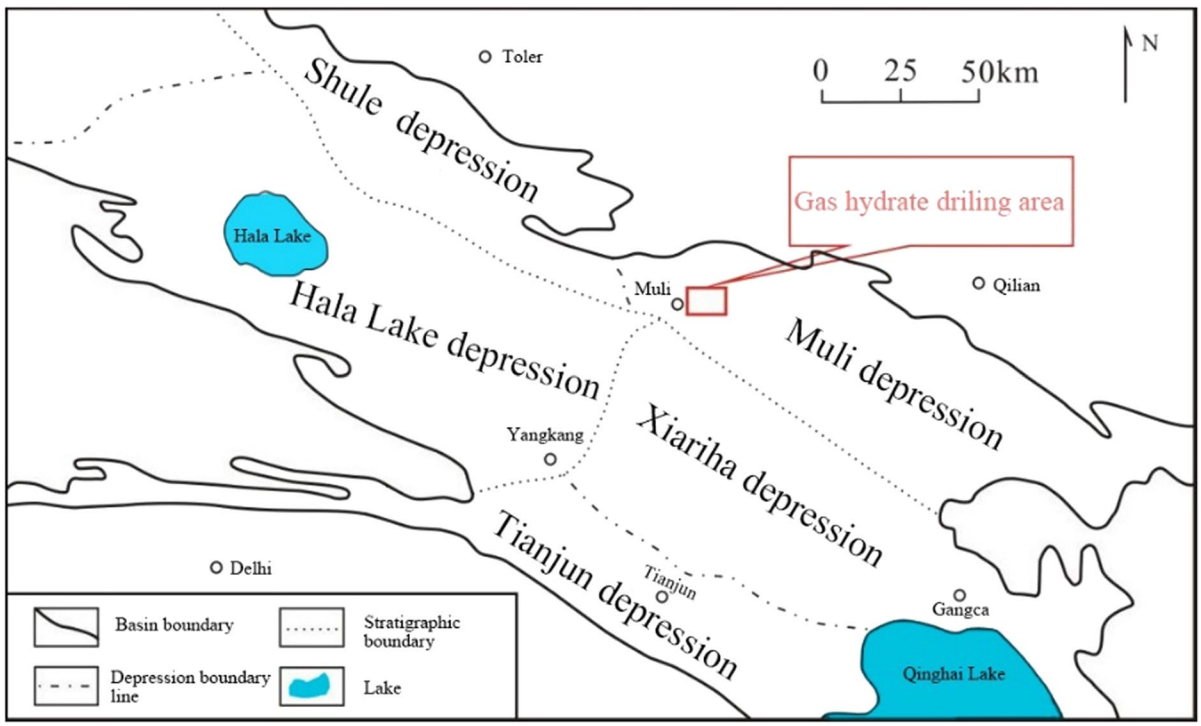

Fig. 6 Sketch map of tectonic units in Qilianshan area, Qinghai Province (Lu et al 2010)

natural gas hydrate in permafrost area of Qilian Mountains, especially in Muli Depression (Zhu et al. 2009). As yet, research on natural gas hydrate reservoirs in the permafrost region of Qilian Mountains mainly focus on geological characteristics, gas source characteristics, logging response characteristics, reservoir-forming conditions and thermophysical properties. However, there are few studies on the evaluation of NGHS in this area, and the prediction of NGHS in the reservoir of this area would be of great significance for the evaluation of natural gas hydrate resource reserves.

The DK-1 scientific drilling test well was drilled on October 18, 2008. Its geographical coordinates are 38°05.591′N, 99°10.260′E, and 4057 m above sea level. The drilling process of this well terminated on November 26, 2008, with a depth of 182.25 m. After that, three new wells of DK-2, DK-3 and DK-4 were drilled in this area, at depths of 645.22 m, 765.01 m, and 466.65 m, respectively, and finally, the total length of the four natural gas hydrate reservoir wells reached 2059.13 m. Among the four wells in Muli Depression of the Qilian Mountains permafrost region, Well DK-1 has the largest hydrate reserves and the most abundant data. We, therefore, chose Well DK-1 to analyze NGHS of this reservoir area using the proposed model. A total of 4 intervals of natural gas hydrate layers were discovered in the entire well section, as listed below: (1) 133.5–135.5 m: natural gas hydrate was found within the pores of fine sandstone, presented as white crystals; (2) 142.9–147.7 m: natural gas hydrate existed in the pores and fissures of argillaceous siltstone as white crystals; (3) 165.3–165.5 m: natural gas hydrate crystals were observed in the fissures of argillaceous siltstone; and (4) 169.0–170.5 m: natural gas hydrate was observed in the pores of siltstone (Zhu et al. 2009).

4.2 Determination of parameters

The 142.9–147.7 m section of Well DK-1, which is the thickest among the four natural gas hydrate layers, is chosen for analysis. The acoustic interval transit time and density of Well DK-1 are collected from the literature written by Guo and Zhu (2011), as shown in Fig. 7. The mineral compositions in this natural gas hydrate reservoir were determined by Wang et al. (2019), as shown in Table 5, indicating that sandstone is the main component in this area.

According to the methods introduced in Sect. 2, the parameters of our proposed model for the 142.9–147.7 m well section of Well DK-1 in the permafrost region of Qilian Mountains are obtained, as shown in Table 6. And the porosity of the reservoir with or without hydrate are shown in Fig. 7.

4.3 Predicted results and analysis

According to the data of gas and water extracted from the samples at depths of 142.90 m, 143.25 m, 143.95 m, 144.30 m, 145.00 m, and 146.05 m of the Well DK-1, the measured saturations were determined based on the material balance equation for comparison. The measured saturations of these six samples are 7.5%, 15.8%, 37%, 37.2%, 38.5%, and 40.3%, respectively, as shown in Fig. 7. The measured saturations of the samples at depths of 142.90 m and 143.25 m are much lower than those of the other four samples. This would be due to that these two samples were collected near the upper border of section of Well DK-1in this reservoir. Therefore, according to the Shc of 8.10% for selecting the calculation models of Mode A or B to evaluate natural gas hydrate in reservoir, the calculation model of Mode A is chosen for the NGHS calculation of the 142.9–143.2 m well section and the calculation model of Mode B is used for the 143.2–147.7 m well section. Using the model parameters given in Sect. 4.2, NGHS for the 142.9–147.7 m well section of Well DK-1 in the permafrost region of Qilian Mountains can be calculated by the proposed model, as shown in Fig. 7.

NGHSs predicted by the proposed model for the 142.9–147.7 m well section of Well DK-1 are in the range of 5.3–54.1%. The errors of the predicted results at well depths of 142.90 m, 143.25 m, 143.95 m, 144.30 m, 145.00 m, and 146.05 m of the Well DK-1 are 9.33%, 13.92%, 10.00%, 10.75%, 9.87%, and 9.18%, respectively, with an average error of 10.56%. This indicates that the proposed model can evaluate NGHS in the reservoir of the Qilian Mountains permafrost region with reasonable accuracy. In addition, the error of NGHS predicted by the model of Mode A is generally lower than those predicted by the model of Mode B, and the error of NGHS predicted by the model of Mode B decreases with increasing measured saturation.

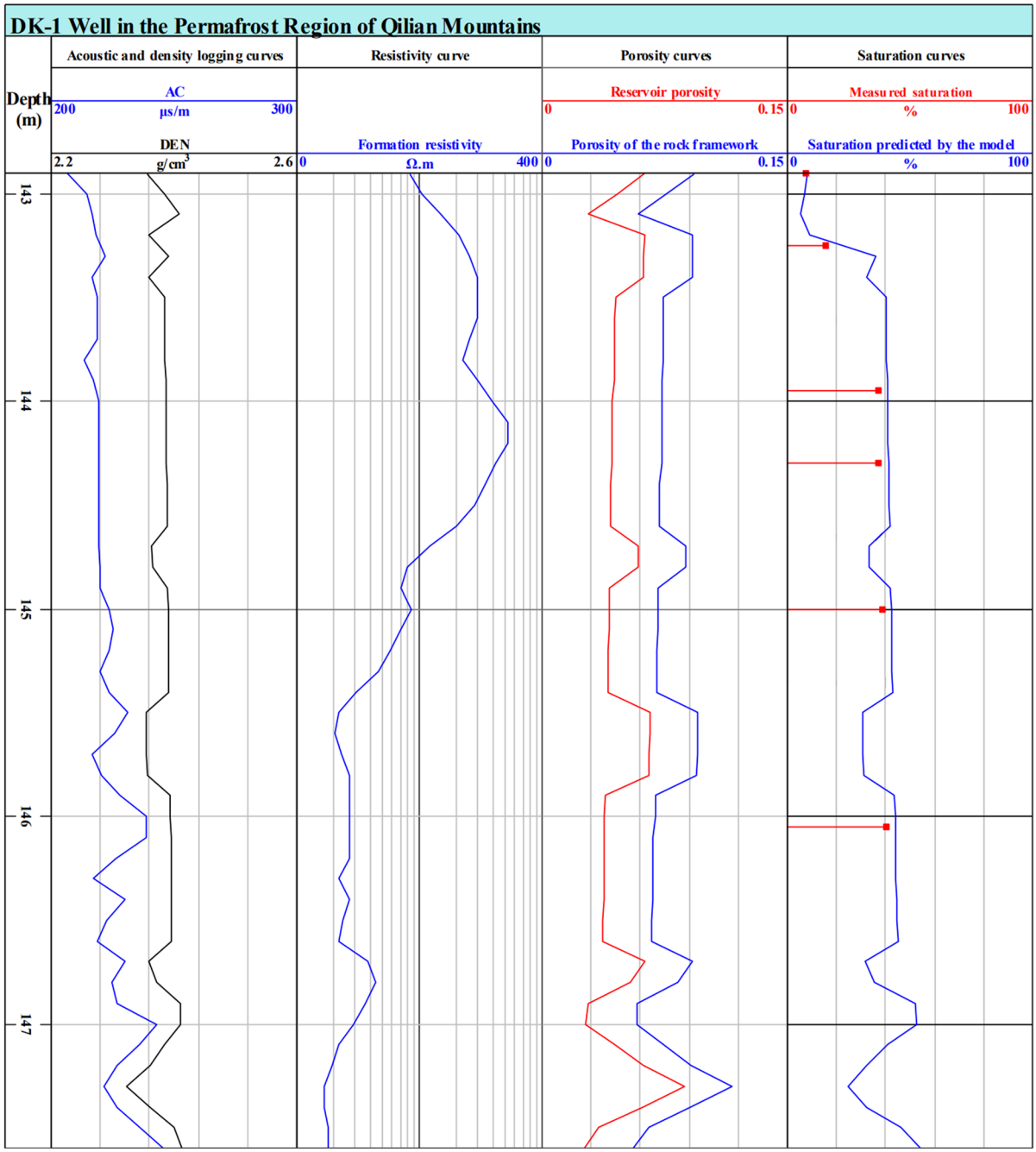

Fig. 7 Logging data, reservoir porosities and natural hydrate saturation for the 142.9–147.7 m well section of Well DK-1 in the permafrost region of Qilian Mountains

The change behavior of prediction error with measured saturation are consistent with the results obtained by the experiments, as shown in Fig. 4a. The reason for this would be that some part of the natural gas hydrate is regarded as water for NGHS calculation using the proposed model of Mode B when the NGHS is relatively low, as mentioned in Sect. 3.4. Furthermore, the length of the analyzed

Table 5 Mineral compositions and the corresponding bulk modulus and shear modulus of the rock in the 142.9–147.7 m section of Well DK-1 in the permafrost region of Qilian Mountains (Wang et al 2019)

Rock compositions	Quaternary sediments	Coal	Shale	Mudstone	Siltstone	Fine sandstone	Medium sandstone	Coarse sandstone
Volume fraction (%)	2.63	7.87	5.43	15.18	48.42	14.93	0.82	4.72
Bulk modulus (MPa)	5.65	1000	5100	9970	24,000	5200	3300	4200
Shear modulus (MPa)	8.74	460	3300	7350	27,000	3600	2500	2900

Table 6 Parameters of the proposed model for the 142.9–147.7 m well section of Well DK-1 in the permafrost region of Qilian Mountains

K_{ma} (MPa)	G_{ma} (MPa)	ρ_m (g/cm^3)	ϕ_c	r	Δt_{mc} (μs/m)	ρ_f (g/cm^3)	σ_{min}	β_1	β_2	ξ	λ (m^{-1})
7350	9165	2.65	0.36	9.5	250	1.03	4.825	0.461	1.081	1.68	0.0002

well section is only 4.8 m, and the difference of the minimum in-situ stress in the vertical two horizontal directions calculated by this proposed model is lower than 0.113 MPa. Therefore, the effect of the stress difference can be ignored resulting in that there is no relation between the error of the predicted results and the depth.

In general, the errors of the predicted results calculated by the proposed model are all lower than 13.92%, with an average value of 10.51%. This indicates that the predicted results are in good agreement with the measured saturations. In addition, the change behavior of the errors of predicted results compared with the measured saturation agrees well with experiment data, as shown in Sect. 3.4, implying that the proposed model has a good consistency for both experimental analysis and engineering application. So, the satisfying performance of the predicted results by the proposed model shows that this new method developed by the equivalent medium theory is suitable for evaluating the NGHS in the permafrost region reservoir. Furthermore, this method can make full use of field well logging data and does not use too much experimental data for parameter determination, which would highly increase its adaptability.

As what have discussed above, the proposed method would be used as a superior guidance for the accurate evaluation of NGHS. By using the proposed method to obtain an accurate NGHS, the natural gas hydrate reserves can be estimated clearly for the gas reservoir development design, as well as, the exploitation degree of a natural gas hydrate reservoir after production can be monitored effectively. And beyond that, NGHS is also an important parameter for the stability analysis of the wellbore in the formation containing natural gas hydrate. The proposed method of NGHS evaluation is beneficial to the drilling design and operation in the natural gas hydrate reservoir. As well as, it is meaningful for the drilling engineering of other oil and gas development when the well goes through the formation containing natural gas hydrate in high latitude or altitude regions. Furthermore, it is impossible to collect the sediment in natural gas hydrate reservoir without any disturbance. In this case, the original NGHS in the reservoir cannot be tested directly using the sediment sample. Fortunately, NGHS can be calculated by the proposed method using logging data, and the logging data can reflect the original situation of the natural gas hydrate reservoir. In general, the novel evaluation method of NGHS presented in this paper is significative for the geological resource exploitation related to the natural gas hydrate stratum.

5 Conclusions

(1) A novel evaluation method of natural gas hydrate saturation (NGHS) in reservoirs is developed in this paper. In light of the equivalent medium theory, the method is derived according to the

concept that the natural gas hydrate is regarded as the fluid (Mode A) when NGHS is relatively low, while as the rock matrix (Mode B) when NGHS is high. And if NGHS is no more than 8.10%, the calculation model of Mode A is used for NGHS evaluation, whereas the calculation model of Mode B is used when NGHS is higher than 8.10%.

(2) The errors of predicted results by the proposed model are lower than 16.4%. The comprehensive error analysis shows that R^2 is 0.968 and AAEPR is 8.90%. And the predictive capability of the proposed model is significantly better than those of Wood equation and Weight equation.

(3) The prediction accuracy of the proposed model is highly affected by triaxial uniform stress, showing that the error of the predicted results generally increases with increasing triaxial uniform stress. As well as, the error of the predicted results for Mode B decreases with increasing measured saturation.

(4) NGHSs predicted by the proposed model for the 142.9–147.7 m well section of Well DK-1 are in the range of 5.3–54.1%. The errors are 9.18–13.92%, with an average error of 10.56%, compared with the measured saturations determined by the material balance equation. And the error of Mode A is generally lower than those predicted by Mode B.

(5) The satisfying performance of the predicted results by the proposed model shows that this method is suitable for evaluating the NGHS of the permafrost region reservoir. This method can make full use of field well logging data and does not use too much experimental data for parameter determination. The novel evaluation method of NGHS presented in this paper is significative for the geological resource exploitation related to the natural gas hydrate stratum.

Acknowledgements The financial supports from the Sichuan Science and Technology Program (No. 2022NSFSC0185), the National Natural Science Foundation of China (Grant Nos. 42172313, 51774246 and U20B6005) are appreciated. The authors would like to express their gratitude to the editors and anonymous reviewers for their constructive comments on the draft paper.

Declarations

Conflict of interest The authors declare that they have no known competing financial interests or personal relationships that could have appeared to influence the work reported in this paper.

References

Alger RP, Raymer LL (1963) Formation density log applications in liquid-filled holes. J Petrol Technol 15(3):321–332. https://doi.org/10.2118/435-PA

Amiri M, Yunan MH, Zahedi G, Jaafar MZ, Oyinloye EO (2012) Introducing new method to improve log derived saturation estimation in tight shaly sandstones-A case study from Mesaverde tight gas reservoir. J Petrol Sci Eng 92–93:92–93. https://doi.org/10.1016/j.petrol.2012.06.014

Archie GE (2003) The electrical resistivity log as an aid in determining some reservoir characteristics. SPE Repr Ser 55:9–16. https://doi.org/10.2118/942054-G

Arun KP, Sain K, Kumar J (2018) Elastic parameters from constrained AVO inversion: application to a BSR in the Mahanadi offshore, India. J Nat Gas Sci Eng 50:90–100. https://doi.org/10.1016/j.jngse.2017.10.025

Azar JH, Javaherian A, Pishvaie MR, Nabi-Bidhendi M (2008) An approach to defining tortuosity and cementation factor in carbonate reservoir rock. J Petrol Sci Eng 60(2):125–131. https://doi.org/10.1016/j.petrol.2007.05.010

Bao X, Luo T, Li H (2022) A prediction method of suspended natural gas hydrate saturation in sea area based on P-wave impedance. Fuel 324:124505. https://doi.org/10.1016/j.fuel.2022.124505

Burland J, Chapman T, Skinner H, Brown M (2012) ICE manual of geotechnical engineering. Proc Inst Civ Eng 165:59. https://doi.org/10.1680/moge.57098

Ding J, Cheng Y, Deng F, Yan C, Sun H, Li Q, Song B (2020) Experimental study on dynamic acoustic characteristics of natural gas hydrate sediments at different depths. Int J Hydrog Energy 45(51):26877–26889. https://doi.org/10.1016/j.ijhydene.2020.06.295

Dvorkin J, Prasad M, Sakai A, Lavoie D (1999) Elasticity of marine sediments: rock physics modeling. Geophys Res Lett 26(12):1781–1784. https://doi.org/10.1029/1999GL900332

Dvorkin J, Helgerud MB, Waite WF, Kirby SH, Nur A (2003) Introduction to physical properties and elasticity models. Nat Gas Hydrate 5:245–260. https://doi.org/10.1007/978-94-011-4387-5_20

Ecker C (2001) Seismic characterization of methane hydrate structures. PhD thesis, Stanford University.

Fang H, Shi K, Yu Y (2022) A state-dependent subloading constitutive model with unified hardening function for gas hydrate-bearing sediments. Int J Hydrog Energy 47(7):4441–4471. https://doi.org/10.1016/j.ijhydene.2021.11.104

Guo X, Zhu Y (2011) Well logging characteristics and evaluation of hydrates in Qilian Mountain permafrost. Geol Bull China 30(12):1868–1873

Helgerud MB, Dvorkin J, Nur A, Sakai A, Collett T (1999) Elastic-wave velocity in marine sediments with gas hydrates: effective medium modeling. Geophys Res Lett 26(13):2021–2024. https://doi.org/10.1029/1999gl900421

Kim GY, Narantsetseg B, Ryu BJ, Yoo DG, Lee JY, Kim HS, Riedel M (2013) Fracture orientation and induced anisotropy of gas hydrate-bearing sediments in seismic chimney-like-structures of the Ulleung Basin, East Sea. Mar Pet Geol 47:182–194. https://doi.org/10.1016/j.marpetgeo.2013.06.001

Kuster GT, Toksoz MN (1974) Velocity and attenuation of seismic waves in two-phase media: part II. Experimental results. Geophysics 39(5):607. https://doi.org/10.1190/1.1440451

Leclaire P, Cohen-Ténoudji F, Aguirre-Puente J (1994) Extension of Biot's theory of wave propagation to frozen porous media. J Acoust Soc Am 96(6):3753–3768. https://doi.org/10.1121/1.411336

Lee MW (2002) Biot-Gassmann theory for velocities of gas hydrate-bearing sediments. Geophysics 67(6):1711–1719. https://doi.org/10.1190/1.1527072

Lee MW (2004) Elastic velocities of partially gas-saturated unconsolidated sediments. Mar Pet Geol 21(6):641–650. https://doi.org/10.1016/j.marpetgeo.2003.12.004

Lee MW, Hutchinson DR, Collett TS, Dillon WP (1996) Seismic velocities for hydrate-bearing sediments using weighted equation. J Geophys Res B Solid Earth 101(9):20347–20358. https://doi.org/10.1029/96jb01886

Li H, Liu J, Qu C, Song H, Zhuang X (2022a) A method for calculating gas hydrate saturation by dual parameters of logging. Front Earth Sci 10:986647. https://doi.org/10.3389/feart.2022.986647

Li N, Sun W, Li X, Feng Z, Wu H, Wang K (2022b) Gas hydrate saturation model and equation for logging interpretation. Pet Explor Dev 49(6):1243–1250. https://doi.org/10.1016/s1876-3804(23)60346-5

Liu X, Luo P (2004) Rock mechanics and petroleum engineering. Petroleum Industry Press, Beijing, p 16

Liu H, Fan X, Tang H (2013) Principle and application of well logging. Petroleum Industry Press, Beijing, p 774

Liu F, Liang J, Lai H, Han L, Wang X, Li T, Wang F (2022) Two-phase modeling technology and subsection modeling method of natural gas hydrate: a case study in the Shenhu Sea Area. Front Earth Sci 10:884375. https://doi.org/10.3389/feart.2022.884375

Lu S, McMechan GA (2004) Elastic impedance inversion of multichannel seismic data from unconsolidated sediments containing gas hydrate and free gas. Geophysics 69(1):164. https://doi.org/10.1190/1.1649385

Lu Z, Zhu Y, Zhang Y, Wen H, Li Y, Jia Z, Liu C, Wang P, Li Q (2010) Basic geological characteristics of gas hydrates in Qilian Mountain permafrost area, Qinghai Province. Miner Depos 29(01):182–191. https://doi.org/10.16111/j.0258-7106.2010.01.003

Nur A, Mavko G, Dvorkin J, Galmudi D (1998) Critical porosity: a key to relating physical properties to porosity in rocks. Lead Edge 17(3):357–362. https://doi.org/10.1190/1.1437977

Pandey L, Sain K (2022) Joint inversion of resistivity and sonic logs using gradient descent method for gas hydrate saturation in the Krishna Godavari offshore basin, India. Mar Geophys Res 43(3):1–12. https://doi.org/10.1007/s11001-022-09491-z

Pearson CF, Halleck PM, McGuire PL (1983) Natural gas hydrate deposits: a review of in situ properties. J Phys Chem 87(21):4180–4185. https://doi.org/10.1021/j100244a041

Poupon A, Loy ME, Tixier MP (1954) A contribution to electrical log interpretation in shaly sands. J Petrol Technol 6(6):27–34. https://doi.org/10.2118/311-G

Priestley K (1999) The rock physics handbook: tools for seismic analysis in porous media. Geol Mag 136(6):709

Qiu Z, Wang J, Huang S, Bai J (2019) Wetting-induced axial and volumetric strains of a sandstone mudstone particle mixture. Mar Georesour Geotechnol 37(1):36–44. https://doi.org/10.1080/1064119X.2018.1425783

Riedel M, Collett TS, Kim HS, Bahk JJ, Kim JH, Ryu BJ, Kim GY (2013) Large-scale depositional characteristics of the Ulleung Basin and its impact on electrical resistivity and Archie-parameters for gas hydrate saturation estimates. Mar Pet Geol 47:222–235. https://doi.org/10.1016/j.marpetgeo.2013.03.014

Shelander D, Dai J, Bunge G, Singh S, Eissa M, Fisher K (2012) Estimating saturation of gas hydrates using conventional 3D seismic data, Gulf of Mexico Joint Industry Project Leg II. Mar Pet Geol 34(1):96–110. https://doi.org/10.1016/j.marpetgeo.2011.09.006

Shen J, Karakus M, Chao Xu (2012a) A comparative study for empirical equations in estimating deformation modulus of rock masses. Mar Pet Geol 32:245–250. https://doi.org/10.1016/j.tust.2012.07.004

Shen J, Priest S, Karakus M (2012b) Determination of Mohr-Coulomb shear strength parameters from generalized Hoek-Brown criterion for slope stability analysis. Rock Mech Rock Eng 45(1):123–129. https://doi.org/10.1007/s00603-011-0184-z

Shen J, Jimenez R, Karakus M, Xu C (2014) A simplified failure criterion for intact rocks based on rock type and uniaxial compressive strength. Rock Mech Rock Eng 47(2):357–369. https://doi.org/10.1007/s00603-013-0408-5

Simandou P (1964) Dielectric measurements in porous media-applications to measurement of water saturation-study

of behavior of blocks of shaly rocks. J Petrol Technol 16(9):1045

Sun Z, Shi J, Zhang T, Wu K, Miao Y, Feng D, Sun F, Han S, Wang S, Hou C (2018) The modified gas-water two phase version flowing material balance equation for low permeability CBM reservoirs. J Petrol Sci Eng 165:726–735. https://doi.org/10.1016/j.petrol.2018.03.011

Wang P, Zhu Y, Lu Z, Bai M, Huang X, Pang S, Zhan S, Liu H, Xiao R (2019) Research progress of gas hydrates in the Qilian Mountain permafrost, Qinghai, northwest China: review. Sci Sin Phys Mech Astron 49(3):034606. https://doi.org/10.1360/sspma2018-00133

Wyllie MRJ, Gregory AR, Gardner GHF (1958) An experimental investigation of factors affecting elastic wave velocities in porous media. Geophysics 23(3):459–493. https://doi.org/10.1190/1.1438493

Yin S, Ding W, Zhou W, Shan Y, Xie R, Guo C, Cao X, Wang R, Wang X (2017) In situ stress field evaluation of deep marine tight sandstone oil reservoir: a case study of Silurian strata in northern Tazhong area, Tarim Basin, NW China. Mar Pet Geol 80:49–69. https://doi.org/10.1016/j.marpetgeo.2016.11.021

Zhang F, Ding L, Yang X (2015) Prediction of pressure between packers of staged fracturing pipe strings in high-pressure deep wells and its application. Nat Gas Ind B 2(2):252–256. https://doi.org/10.1016/j.ngib.2015.07.018

Zhang Q, Wang Z, Fan X, Wei N, Zhao J, Lu X, Yao B (2021a) A novel mathematical method for evaluating the wellbore deformation of a diagenetic natural gas hydrate reservoir considering the effect of natural gas hydrate decomposition. Nat Gas Ind B 8:287–301. https://doi.org/10.1016/j.ngib.2021.04.009

Zhang Q, Yao B, Fan X, Li Y, Li M, Zeng F, Zhao P (2021b) A modified Hoek-Brown failure criterion for unsaturated intact shale considering the effects of anisotropy and hydration. Eng Fract Mech 241:107369. https://doi.org/10.1016/j.engfracmech.2020.107369

Zhang Q, Yao B, Fan X, Li Y, Fantuzzi N, Ma T, Chen Y, Zeng F, Li X, Wang L (2023) A failure criterion for shale considering the anisotropy and hydration based on the shear slide failure model. Int J Min Sci Technol 33:447–462. https://doi.org/10.1016/j.ijmst.2022.10.008

Zhao J, Ji Y, Wu Y (2018) Reliability experiment on the calculation of natural gas hydrate saturation using acoustic wave data. Nat Gas Ind B 5(4):293–297. https://doi.org/10.1016/j.ngib.2017.12.008

Zhu Y, Zhang Y, Wen H, Lu Z, Jia Z, Li Y, Li Q, Liu C, Wang P, Guo X (2009) Discovery of natural gas hydrate in the permafrost region of Qilian Mountains, Qinghai. Acta Geol Sin 83(11):1762–1771

Zhu L, Wu S, Zhou X, Cai J (2023) Saturation evaluation for fine-grained sediments. Geosci Front 14(4):101540. https://doi.org/10.1016/j.gsf.2023.101540

Zhuo L, Yu J, Zhang H, Zhou C (2021) Influence of horizontal well section length on the depressurization development effect of natural gas hydrate reservoirs. Nat Gas Ind B 8(5):505–513. https://doi.org/10.1016/j.ngib.2021.08.007

Zillmer M (2006) A method for determining gas-hydrate or free-gas saturation of porous media from seismic measurements. Geophysics 71(3):21. https://doi.org/10.1190/1.2192910

Zimmerman RW, King MS (1986) Effect of the extent of freezing on seismic velocities in unconsolidated permafrost. Geophysics 51(6):1285–1290. https://doi.org/10.1190/1.1442181